Photoactivity of Mono- and Dicarbonyl Complexes of Ruthenium(II) Bearing an N,N,S-Donor Ligand: Role of Ancillary Ligands on the Capacity of CO Photorelease

Margarita A. Gonzalez,[†] Samantha J. Carrington,[†] Indranil Chakraborty,[†] Marilyn M. Olmstead,[‡] and Pradip K. Mascharak*,[†]

[†]Department of Chemistry and Biochemistry, University of California, Santa Cruz, California 95064, United States
[‡]Department of Chemistry, University of California, Davis, California 95616, United States

S *Supporting Information*

ABSTRACT: One monocarbonyl and one dicarbonyl complex of ruthenium(II), namely, $[Ru(Cl)(CO)(qmtpm)(PPh_3)]BF_4$ (**2**) and $[Ru(Cl)(CO)_2(qmtpm)]ClO_4$ (**3**), derived from the tridentate ligand 2-quinoline-*N*-(2′-methylthiophenyl)-methyleneimine (qmtpm) have been synthesized and structurally characterized. The qmtpm ligand binds in a meridional fashion in these carbonyl complexes, and in **3**, the two carbon monoxide (CO) ligands are cis to each other. Solutions of **2** in ethanol, chloroform, or acetonitrile rapidly release CO upon illumination with low-power (3–15 mW) light in the 300–450 nm range. Loss of CO from **2** brings about a dramatic color change from yellow to magenta because of the formation of $[Ru(Cl)(MeCN)(qmtpm)(PPh_3)]BF_4$ (**4**). In acetonitrile, photorelease of CO from **3** under 360 nm light occurs in two steps, and the violet photoproduct $[Ru(Cl)(MeCN)_2(qmtpm)]^+$ upon reaction with Ag^+ and PPh_3 affords red $[Ru(MeCN)_2(qmtpm)(PPh_3)](ClO_4)_2$ (**5**). The structure of **5** has also been determined by X-ray crystallography. Reduced myoglobin assay confirms that **2** and **3** act as photoactive CO-releasing molecules (photoCORMs) that deliver 1 and 2 equiv of CO, respectively. The results of density functional theory (DFT) and time-dependent DFT studies confirm that electronic transitions from molecular orbitals with predominantly Ru−CO character to ligand-based π^* orbitals facilitate CO release from these two photoCORMs. Complexes **2**−**5** have provided an additional opportunity to analyze the roles of the ancillary ligands, namely, PPh_3, Cl^-, and MeCN, in shifting the positions of the metal-to-ligand charge-transfer bands and the associated sensitivity of the two photoCORMs to different wavelengths of light. Collectively, the results provide helpful hints toward the future design of photoCORMs that release CO upon exposure to visible light.
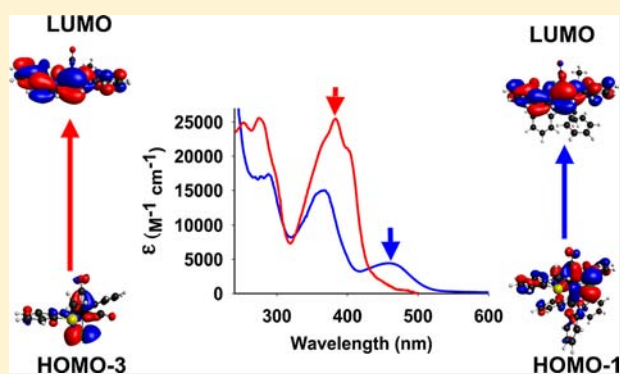
■ INTRODUCTION

Carbon monoxide (CO) is endogenously produced during the breakdown of heme proteins by either inducible or constitutive forms of the enzyme heme oxygenase (HO).[1] Although the details of HO action has been known for some time, CO was initially dismissed as a metabolic waste product. Focus on the anti-inflammatory properties of the bile pigments biliverdin and bilirubin[2] (generated in the later stages of heme catabolism) has, however, led to important insights regarding HO activity in anti-inflammatory responses. It was not until the past decade that the role of endogenously produced CO was reassessed and implicated in physiological processes such as vasodilation,[3] antiapoptotic activity,[4] and cell signaling.[5] CO mediates cell protection by interacting with heme-containing metalloproteins in stress response pathways, thus earning its reputation as a cytoprotective agent. For instance, inhibition of mitochondrial cytochrome *c* by both exogenously and endogenously produced CO has been found to precondition neuronal cells against apoptosis.[6] Indeed, increased CO levels associated with HO

upregulation has been noted in cases of ischemia/reperfusion injury,[7] aid of organ graft survival,[8] modulation of inflammatory conditions such as lung injury,[9] and myocardial infarction.[10]

While exogenous CO gas application has shown promise in animal models of transplantation,[11] site-specific delivery of this toxic gas is imperative to effectively induce the benefits of CO-mediated protection and to circumvent toxicity associated with asphyxiation. In recent years, CO complexes bearing low-valent metal centers have been studied as photoactive CO-releasing molecules (photoCORMs) because of the inherent photo-sensitivity of metal carbonyl complexes.[12,13] The initial photoCORMs reported underwent UV-light-triggered CO release because metal−CO bonds typically require high energies for dissociation owing to strong back-bonding interactions. For example, near-UV photolysis of the water-soluble salt $Na_3[W(CO)_5(TPPTS)]$ [TPPTS = tris-

(sulfonatophenyl)phosphine trianion] resulted in 1.2–1.6 mol of CO per molecule of CORM released.[14] The presence of CO groups in the autoxidation product suggests that not all metal–CO bonds are labilized. Similarly, UV light was required for CO delivery from the iron carbonyl complex [Fe(CO)(N4Py)]-(ClO₄)₂ [N4Py = pentadentate tetrakis(pyridine) ligand].[15] A particular subset of photoCORMs consists of *fac*-manganese(I) tricarbonyl complexes, wherein a low-valent manganese center is stabilized by a tripodal ligand and three CO groups. Schatzschneider and co-workers reported [Mn(CO)₃(tpm)]-PF₆, the first in this series,[16] and have since expanded their set of tripodal ligands to include imidazole moieties and their derivatives.[17] For this subgroup of photoCORMs, exhaustive UV photolysis affords three CO ligands per molecule and a bridged μ-OMn^{III} compound as the final photoproduct.[18]

We have been interested in the nature of electronic transition(s) in metal carbonyl complexes that promotes CO photolability in the visible and near-infrared (NIR) region. As part of such effort, we have recently demonstrated that, for manganese(I) tricarbonyl complexes of the composition *fac*-[Mn(L)(CO)₃] (L = tridentate ligands), increased conjugation in the ligand frame L results in a systematic increase in the absorptivity of the corresponding complexes in the longer-wavelength region.[19] For example, the carbonyl complex *fac*-[Mn(pqa)(CO)₃]ClO₄ [where pqa = (2-pyridylmethyl)(2-quinolylmethyl)amine], which features both pyridine and quinoline moieties (Figure 2) in the ligand frame, exhibits a strong absorption band with λ_{max} at 360 nm, while *fac*-[Mn(dpa)(CO)₃]ClO₄ [where dpa = N,N-bis(2-pyridylmethyl)amine, the same ligand frame with two pyridine moieties] displays a weaker band at 350 nm. In another study, we have utilized the ligand 2-quinoline-N-(2′-methylthiophenyl)methyleneimine (qmtpm; Figure 1) to
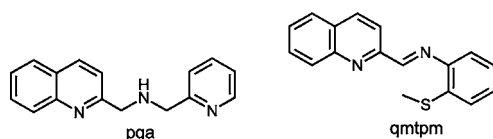
visible region.[20] The results of density functional theory (DFT) studies reveal that inclusion of an –SMe group on the qmtpm frame and a σ-donating Br⁻ ligand leads to enhanced CO photolability by promoting MLCT interactions that weaken the affinity of the metal center toward CO in these photoCORMs.

Although photoCORMs like *fac*-[Mn(pqa)(CO)₃]ClO₄ are quite stable in biologically relevant media, complexes like *fac*-[Mn(Br)(qmtpm)(CO)₃] exhibit lower stability because of the bidentate mode of coordination of the qmtpm ligand (Figure 2). The rigidity arising from inclusion of the imine functionality in the ligand frame does not allow the thioether group to participate in coordination in the *fac*-manganese(I) tricarbonyl complexes derived from qmtpm. As part of our effort to establish ligand design strategies for the isolation of photo-CORMs, we now report the syntheses, structures, and photochemical properties of the two stable ruthenium(II) carbonyl complexes derived from qmtpm in which the ligand coordinates in a *tridentate* fashion. Carbonylation of [Ru-(Cl)₂(qmtpm)(PPh₃)] (1) in ethanol in the presence of Ag⁺ ion yields the monocarbonyl complex [Ru(Cl)(CO)(qmtpm)-(PPh₃)]BF₄ (2), while reaction of [Ru(Cl)₂(CO)₃]₂ with qmptm in boiling methanol affords the dicarbonyl complex [Ru(Cl)(CO)₂(qmtpm)]ClO₄ (3) in high yield. In both of these complexes, the qmtpm ligand binds in a *meridional* fashion, and in 3, the two CO ligands are cis to each other. Complete photolysis of 2 in coordinating solvents such as acetonitrile yields one CO per molecule and forms the solvato species [Ru(Cl)(MeCN)(qmtpm)(PPh₃)]BF₄ (4), which upon reaction with AgClO₄ in acetonitrile affords [Ru-(MeCN)₂(qmtpm)(PPh₃)](ClO₄)₂ (5). The structures of 2, 3, and 5 are reported in this account. In addition, DFT and time-dependent DFT (TDDFT) calculations have been performed to examine the role of MLCT transitions in metal–CO bond labilization in 2 and 3. The results described below strongly suggest that electronic transitions from molecular orbitals (MOs) with predominantly Ru–CO character to ligand-based π^* orbitals facilitate CO release from these two photoCORMs.

■ EXPERIMENTAL SECTION

Materials and Reagents. [Ru(Cl)₂(CO)₃]₂ was purchased from Sigma Aldrich and used as received. The other starting salt [Ru(Cl)₂(PPh₃)₃][21] and the ligand 2-quinoline-N-(2′-methylthiophenyl)methyleneimine (qmtpm)[22] were synthesized following literature procedures. Solvents were purified and/or dried by standard techniques prior to use.

Caution! Transition-metal perchlorates should be prepared in small quantities and handled with great caution as metal perchlorates may explode upon heating.

[Ru(Cl)₂(qmtpm)(PPh₃)] (1). A batch of 0.741 g (0.77 mmol) of [Ru(Cl)₂(PPh₃)₃] and 0.221 g (0.77 mmol) of qmtpm were added to 20 mL of degassed toluene, and the red-brown slurry was heated to reflux for 4 h. The solution turned blue, and a deep-blue solid separated from the solution. The solid was filtered and washed several times with diethyl ether. After thorough drying, this procedure afforded 1 in analytically pure form (also confirmed by its IR, NMR, and electronic absorption spectra (EAS) spectra). Yield: 510 mg (93%). Anal. Calcd for C₃₅H₂₉N₂RuCl₂SP: C, 58.98; H, 4.10; N, 3.93. Found: C, 58.83; H, 4.20; N, 3.91. Selected IR frequencies (KBr disk, cm⁻¹): 1615 (w), 1593 (w), 1519 (m), 1481 (m), 1434 (m), 1090 (m), 827 (w), 787 (w), 753 (m), 697 (s), 525 (s). EAS [CH₂Cl₂; λ_{max}, nm (ε, M⁻¹ cm⁻¹)]: 280 (19226), 355 (17630), 615 (4235). ¹H NMR (CDCl₃, 500 MHz, TMS): δ 10.50 (d, 1H), 9.37 (s, 1H), 7.80 (t, 1H), 7.61 (t, 1H), 7.51 (d, 1H), 7.44 (t, 3H), 7.15–7.24 (m, 8H), 7.02 (t, 3H), 6.88 (t, 6H), 6.54 (t, 1H), 3.11 (s, 3H).

investigate the influence of both a thioether moiety and an imine functionality on the absorption characteristics of the resulting *fac*-[Mn(L)(CO)₃] complexes. The low affinity of the Mn^I center toward thioether donors, however, resulted in the *bidentate* mode of coordination of qmtpm to the Mn^I center in the resulting carbonyl complexes. Nevertheless, the two carbonyl complexes *fac*-[Mn(qmtpm)(MeCN)(CO)₃]ClO₄ (Figure 2) and *fac*-[Mn(Br)(qmtpm)(CO)₃] exhibit strong metal-to-ligand charge-transfer (MLCT) bands at 435 and 535 nm, respectively, and photorelease CO upon illumination in the
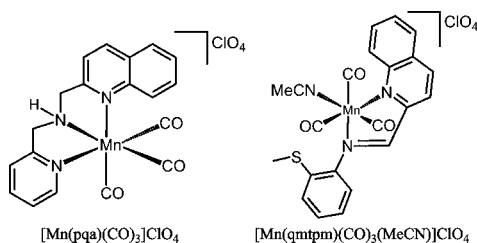

Figure 1. Structures of the ligands.

Figure 2. Structures of the Mn^I photoCORMs.

Table 1. Summary of Crystal Data, Intensity Collection, and Refinement Parameters for 2·H₂O, 3, and 5

	2	3	5
empirical formula	$C_{36}H_{31}BClF_4N_2O_2PRuS$	$C_{19}H_{14}Cl_2N_2O_6RuS$	$C_{39}H_{35}Cl_2N_4O_8PRuS$
fw	809.99	570.35	922.71
cryst color	brown plates	yellow plates	red blocks
cryst size (mm³)	$0.44 \times 0.26 \times 0.07$	$0.40 \times 0.30 \times 0.08$	$0.12 \times 0.11 \times 0.04$
temperature (K)	90(2)	296(2)	296(2)
wavelength (Å)	0.71073	0.71073	0.71073
cryst syst	orthorhombic	monoclinic	triclinic
space group	$P2_12_12_1$	$P2_1/c$	$P\bar{1}$
a (Å)	9.824(2)	13.8529(6)	11.4409(18)
b (Å)	15.179(3)	9.3341(4)	11.936(2)
c (Å)	23.333(6)	16.2461(7)	16.993(3)
α (deg)	90.00	90.00	79.84(2)
β (deg)	90.00	95.6850(10)	84.16(2)
γ (deg)	90.00	90.00	70.16(2)
V (Å³)	3479.4(13)	2090.36(16)	2146.4(6)
Z	4	4	2
d_{calcd} (g/cm³)	1.546	1.812	1.428
μ (mm⁻¹)	0.691	1.146	0.629
GOF^a on F^2	1.149	1.041	1.114
final R indices $[I > 2\sigma(I)]^b$	R1 = 0.0291, wR2 = 0.0689	R1 = 0.0326, wR2 = 0.0697	R1 = 0.0641, wR2 = 0.1889
R indices (all data)^c	R1 = 0.0321, wR2 = 0.0711	R1 = 0.0510, wR2 = 0.0779	R1 = 0.0940, wR2 = 0.2072

^{a}GOF = $[\sum w(|F_o|^2 - |F_c|^2)^2/(N_o - N_v)]^{1/2}$ (N_o = number of observations; N_v = number of variables). ^{b}R1 = $\sum||F_o| - |F_c||/\sum|F_o|$. ^{c}wR2 = $[(\sum w(|F_o|^2 - |F_c|^2)^2/\sum w|F_o|^2)]^{1/2}$.

[Ru(Cl)(CO)(qmtpm)(PPh₃)]BF₄ (2). A slurry of 0.122 g (0.17 mmol) of **1** in 15 mL of ethanol was treated with 1.1 equiv of AgBF₄ (0.037g, 0.19 mmol) to obtain a magenta solution, which was degassed by a freeze−pump−thaw technique. The reaction mixture was allowed to stir for 12 h at room temperature and subsequently heated to reflux under nitrogen for 1 h. The resulting purple reaction mixture was filtered through a Celite pad. A steady stream of CO gas was bubbled through the filtrate for a period of 15 min, during which the color changed from purple to brown and a solid precipitated from the solution. The brown solid was collected by filtration and washed several times with diethyl ether. Yield: 80 mg (59%). Anal. Calcd for $C_{36}H_{29}N_2RuClBF_4OSP$: C, 53.51; H, 3.62; N, 3.47. Found: C, 53.57; H, 3.60; N, 3.39. Selected IR frequencies (KBr disk, cm⁻¹): 2028 (vs, ν_{CO}), 1637 (w), 1516 (w), 1480 (w), 1436 (m), 1084 (s, ν_{BF_4}), 839 (w), 759 (m), 748 (m), 698 (m), 520 (m). EAS [CH_2Cl_2; λ_{max}, nm (ε, M⁻¹ cm⁻¹)]: 292 (15900), 370 (14350), 465 (5310). ¹H NMR (CDCl₃, 500 MHz, TMS): δ 9.92 (d, 1H), 9.61 (s, 1H), 8.52 (d, 1H), 8.34 (d, 1H), 8.14 (t, 1H) 7.96 (t, 1H), 7.80 (m, 2H), 7.47 (s, 1H), 7.28 (t, 7H), 7.20 (t, 3H), 7.04 (t, 5H), 3.08 (s, 3H).

[Ru(Cl)(CO)₂(qmtpm)]ClO₄ (3). A batch of 0.167 g (0.326 mmol) of $[Ru(Cl)_2(CO)_3]_2$ was heated to reflux in 7 mL of methanol to generate a pale-yellow solution. Separately, a slurry of 0.183 g (0.656 mmol) of the qmtpm ligand in 10 mL of methanol was added to a hot solution of $[Ru(Cl)_2(CO)_3]_2$. The resulting red-orange solution was heated to reflux under a N₂ atmosphere for 5 h. Next the volume was reduced to 5 mL under reduced pressure, and the orange solid that separated from the solution was filtered. To the filtrate was added 1 equiv of NaClO₄ (0.043 g, 0.348 mmol), and the mixture was stirred at room temperature for 30 min, during which complex **3** precipitated from the solution as an orange-yellow solid. Yield: 112 mg (60%). Anal. Calcd for $C_{19}H_{14}N_2RuCl_2O_6S$: C, 40.01; H, 2.47; N, 4.91. Found: C, 40.10; H, 2.48; N, 4.88. Selected IR frequencies (KBr disk, cm⁻¹): 2086 (s, ν_{CO}), 2038 (s, ν_{CO}), 1634 (w), 1514 (w), 1434 (w), 1296 (w), 1121 (m), 1083 (s, ν_{ClO_4}), 825 (w), 759 (w), 623 (w), 505 (w). EAS [acetonitrile; λ_{max}, nm (ε, M⁻¹ cm⁻¹)]: 252 (25350), 275 (25700), 385 (25100), 405 (sh, 20770). ¹H NMR (CD₃CN, 500 MHz, TMS): δ 9.76 (d, 1H), 8.92 (d, 1H), 8.42–8.47 (q, 1H), 8.40 (t, 1H), 8.26 (d, 2H), 8.22 (t, 1H), 7.96–8.01 (m, 2H), 7.82 (t, 1H), 3.13 (s, 2H), 3.02 (s, 1H).

[Ru(MeCN)₂(qmtpm)(PPh₃)](ClO₄)₂ (5). To a batch of 0.051 g (0.71 mmol) of **1** in 8 mL of acetonitrile was added 2 equiv of AgClO₄ (0.031 g, 0.150 mmol) dissolved in 7 mL of acetonitrile. The resulting magenta solution was degassed and stirred at room temperature for 12 h, during which a deep-red color developed. The solution was filtered through a Celite pad, and the filtrate was allowed to evaporate slowly to obtain red blocks of **5** suitable for X-ray diffraction. Yield: 40 mg (61%). Anal. Calcd for $C_{39}H_{35}N_4RuCl_2O_8SP$: C, 50.76; H, 3.82; N, 6.07. Found: C, 50.72; H, 3.91; N, 6.06. Selected IR frequencies (KBr disk, cm⁻¹): 1618 (w), 1592 (w), 1435 (w), 1094 (s, ν_{ClO_4}), 757 (w), 698 (w), 623 (m), 530 (m). EAS [CH_3CN; λ_{max}, nm (ε, M⁻¹ cm⁻¹)]: 270 (17125), 310 (14240), 368 (15500), 495 (5400). ¹H NMR (CD₃CN, 500 MHz, TMS): δ 9.56 (s, 1H), 8.60 (d, 1H), 8.55 (d, 1H), 8.13 (d, 1H), 8.01 (d, 1H), 7.95 (t, 1H), 7.85 (m, 2H), 7.61 (d, 1H), 7.47–7.52 (m, 2H), 7.22 (m, 3H), 7.06 (m, 15H), 2.90 (s, 3H), 2.69 (s, 3H).

Physical Measurements. ¹H NMR spectra were recorded at 298 K on a Varian Unity Inova 500 MHz instrument. A Perkin-Elmer Spectrum One Fourier transform infrared sepctrometer was utilized to monitor the IR spectra of the compounds. Electronic absorption spectrometry (EAS) spectra were obtained on a Varian Cary 50 spectrophotometer. Room temperature magnetic susceptibility measurements were performed with a Johnson Matthey magnetic susceptibility balance.

Photolysis Experiments. For continuous-wave photolysis experiments, the light source was an IL-410 illuminator (Electro FiberOptics Corp.) equipped with various light filters. The power of the incident light was measured with a Field MaxII-TO laser power meter (from Coherent, Portland, OR). The rates of CO photorelease were measured by recording the EAS spectra of **2** and **3** in acetonitrile and ethanol (both 0.25 mM, 1.4 mL) and monitoring either the loss of absorbance at 460 nm (for **2**) or the rise in absorbance of the 565-nm charge-transfer band (for **3**) of samples exposed to light at definite time intervals. The plots were fitted to the three-parameter exponential equation $A(t) = A_\infty + (A_o - A_\infty)\exp(-k_{CO}t)$, where A_o and A_∞ are the initial and final absorbance values, respectively. The apparent rates of CO loss (k_{CO}) were calculated from the $\ln(C)$ versus time (T) plot for each compound.

The quantum yield (ϕ) values of CO release were determined by using a Newport Oriel Apex Illuminator (150 W xenon lamp)

equipped with an Oriel 1/8m Cornerstone monochromator. Standard ferrioxalate actinometry[23] was used to determine the quantum yields at 436 nm (for **2**) and 392 nm (for **3**). Solutions of **2** and **3** were prepared under dim-light conditions and placed in a 2 mm × 10 mm quartz cuvette, 2 cm away from the light source. Solutions were prepared to ensure sufficient absorbance (>90%) at the irradiation wavelength, and changes in the EAS spectra in the 460 and 565 nm regions (<10% photolysis) were used to determine the extent of CO release.

Myoglobin Assay. Horse heart myoglobin was dissolved in phosphate-buffered saline (100 mM, pH 7.4) and reduced by adding sodium dithionite. The concentration of the resulting deoxymyoglobin (Mb) was calculated from the absorbance of the Soret band at 435 nm (extinction coefficient = 121 mM^{-1} cm^{-1}). Because sodium dithionite is known to facilitate the release of CO,[24] an apparatus was constructed using two quartz cuvettes. In the first cuvette under anaerobic conditions, the photoactive complexes were exposed to light evolving CO into the headspace. The photogenerated CO was then transferred into the second cuvette containing the reduced Mb solution via a cannula by a positive pressure of N$_2$(g), and the absorbance was taken after 5 min to ensure complete capture of the photoreleased CO. Conversion of Mb to carbonyl myoglobin (Mb-CO) was monitored at defined time intervals. A shift in λ_{max} from 435 to 424 nm was noted in each case because of the formation of Mb-CO. Final concentrations of Mb-CO were assessed at 424 nm (extinction coefficient = 207 mM^{-1} cm^{-1}) and compared to the initial Mb present in solution to quantify the amount of CO released by each compound.

X-ray Crystallography. X-ray-quality crystals of brown plates of **2** were grown by diffusion of pentane into a dilute solution of the complex in dichloromethane. Yellow plates of **3** were obtained by diffusion of toluene into an acetonitrile solution. Diffraction data were collected on a Bruker APEX-II instrument using monochromated Mo Kα radiation (λ = 0.71073 A). The data for **2** were collected at 90 K, while for **3** and **5**, the data collection temperature was 296 K. All data were corrected for absorption, and the structures were solved by direct methods using the *SHELXTL* (1995−1999) software package (Bruker Analytical X-ray Systems Inc.). Additional refinement details are contained in the CIF files (Supporting Information). Crystal data, instrument, and data collection parameters are summarized in Table 1. Selected bond distances and angles are listed in Table 2.

DFT and TDDFT Calculations. DFT and TDDFT studies were executed with the *PC-GAMESS* program[25] using the hybrid functional PBE0. DFT calculations were carried out using the double-ζ basis set 6-31G* for all atoms except ruthenium, for which the quasi-relativistic Stüttgart−Dresden effective core potential was implemented. The X-ray crystal structure coordinates of complexes **2**, **3**, and **5** were used as a starting point for the gas-phase geometry optimization. Electronic transition energies and oscillator strengths were then calculated for **2**−**5** at their PBE0-optimized geometries using TDDFT. For each compound, the 20 lowest-energy electronic excitations were calculated and the solvent effect was added using the polarized continuum model[26] and ethanol as the solvent. The calculated MOs were visualized with the aid of *MacMolPlt*.[27]

■ SYNTHESES AND INTERCONVERSIONS

The reaction of [Ru(Cl)$_2$(PPh$_3$)$_3$] with qmtpm in toluene at refluxing temperature afforded **1** in good yield. The composition of this complex was established with the aid of microanalytical data and its ^{1}H NMR spectrum in CDCl$_3$. The singlet observed at 3.11 ppm confirms S-ligation of qmtpm to the Ru^{II} center in **1**. In free qmtpm, the −SMe signal is noted at 2.52 ppm. Integration of the proton resonances indicates the presence of one PPh$_3$ ligand, while the other two coordination positions are occupied by the two Cl$^-$ ligands. We have tentatively assigned a cis disposition to the two Cl$^-$ ligands in **1** on the basis of the crystal structure of the related complex [Ru(Cl)$_2$(pmtpm)(PPh$_3$)] [where pmtpm = 2-pyridyl-N-(2′-methylthiophenyl)methyleneimine].[28]

Table 2. Selected Bond Distances (Å) and Angles (deg) for 2, 3, and 5

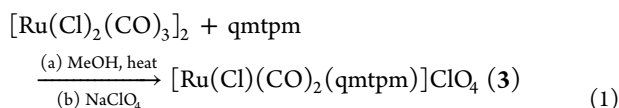|	2	3	5
Ru−N1	2.1633(18)	2.1305(19)	2.155(5)
Ru−N2	2.0190(19)	2.060(2)	2.017(2)
Ru−S1	2.3166(6)	2.3357(7)	2.3137(18)
Ru−C1	1.923(2)	1.903(3)	
Ru−C2		1.890(3)	
Ru−P1	2.4719(7)		2.3485(19)
Ru−Cl1	2.4352(6)	2.4176(7)	
Ru−N4			2.056(6)
Ru−N3			2.087(6)
C1−O1	1.127(3)	1.137(3)	
C2−O2		1.130(3)	
C1−Ru−P1	175.70(6)		
Cl1−Ru−P1	90.27(2)		
Cl1−Ru−N2	176.11(5)	86.21(6)	
N1−Ru−S1	163.22(5)	161.32(6)	162.87(15)
C1−Ru−S1	92.31(7)	93.45(8)	
C1−Ru−N2	93.44(8)	171.24(10)	
C2−Ru−S1		95.99(8)	
C1−Ru−C2		94.71(11)	
N2−Ru−S1	84.75(5)	83.96(6)	85.29(15)
N2−Ru−N1	78.48(7)	78.13(8)	77.9(2)
Cl1−Ru−C2		179.13(8)	
Cl1−Ru−C1	85.58(6)	85.22(8)	
Cl1−Ru−N1	105.25(5)	88.64(6)	
Cl1−Ru−S1	91.53(2)	84.88(2)	
P1−Ru−N3			176.21(16)
N4−Ru−N2			176.4(2)
P1−Ru−N2	90.63(5)		91.92(15)
P1−Ru−N1	92.88(5)		94.12(14)
P1−Ru−S1	86.67(2)		89.89(7)
N1−Ru−N4			104.7(2)
C1−Ru−N1	89.30(8)	103.47(10)	
N1−Ru−C2		90.53(9)	
N2−Ru−C2		93.89(10)	
N1−Ru−N3			84.5(2)
N2−Ru−N3			91.2(2)
N3−Ru−S1			92.46(16)
N4−Ru−S1			91.89(17)
N4−Ru−P1			90.24(16)
N4−Ru−N3			86.7(2)
Ru−C1−O1	173.7(2)	173.4(32)	
Ru−C2−O2		175.6(2)	

In the present work, complex **1** was synthesized for its potential use as the starting material for mono- and dicarbonyl species. However, attempts to replace the Cl$^-$ ligands of **1** with CO led to very different results depending on the solvent. For example, in acetonitrile, heating with 1 equiv of AgBF$_4$ generated the magenta complex **4** (Scheme 1). The further addition of 1 equiv of AgBF$_4$ afforded the red complex [Ru(MeCN)$_2$(qmtpm)(PPh$_3$)]$^{2+}$ (Scheme 1), which has been structurally characterized as the perchlorate salt **5**. Bubbling of CO gas to such solutions did *not* yield either the monocarbonyl complex **2** or [Ru(CO)$_2$(qmtpm)(PPh$_3$)]$^{2+}$, the expected dicarbonyl species. In contrast, the treatment of **1** with Ag$^+$ salts in boiling ethanol followed by passage of a steady stream of CO gas at room temperature led to the replacement of one Cl$^-$, as evidenced by formation of the brown monocarbonyl

Scheme 1
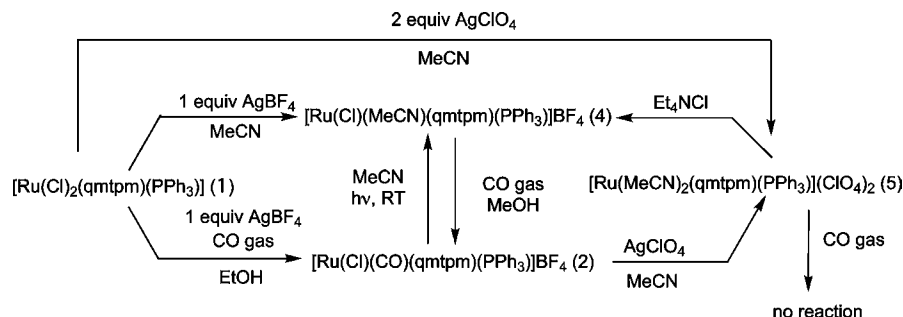
complex **2** (Scheme 1). It is important to note that even in ethanol *only one* Cl⁻ can be exchanged with CO. Collectively, these reactions indicate that acetonitrile is a better donor for the Ru^II center, and any replacement of the Cl⁻ ligand of **1** with CO is possible only in hot ethanol. The affinity of the Ru^II center toward acetonitrile is further indicated by the quantitative formation of **5** upon reaction of **2** with 1 equiv of Ag⁺ salts in hot acetonitrile (Scheme 1).

Success in the isolation of the dicarbonyl complex *cis*-**3** was achieved when $[Ru(Cl)_2(CO)_3]_2$ was employed as the starting salt. In a boiling methanolic solution, the chloro-bridged dimeric carbonyl was allowed to react with qmtpm to afford **3** (as a perchlorate salt) in good yield (eq 1). The reaction presumably proceeds through the solvent-assisted bridge cleavage of $[Ru(Cl)_2(CO)_3]_2$,[29] followed by coordination of qmtpm to the Ru^II center. Interestingly, the reaction of the dicarbonyl precursor *cis*-$[Ru(Cl)_2(CO)_2(PPh_3)_2]$[21] with qmtpm in solvents such as methanol, toluene, chloroform, and acetonitrile did not afford **3**.

$$[Ru(Cl)_2(CO)_3]_2 + qmtpm$$

$$\xrightarrow[\text{(b) NaClO}_4]{\text{(a) MeOH, heat}} [Ru(Cl)(CO)_2(qmtpm)]ClO_4 \ (3) \qquad (1)$$

Structures of the Complexes. 2. The structure of the cation of **2** is shown in Figure 3, and selected metric parameters are listed in Table 2. The ruthenium center in this carbonyl complex resides in an octahedral environment, with the qmtpm ligand coordinated in a meridional fashion. The bulky
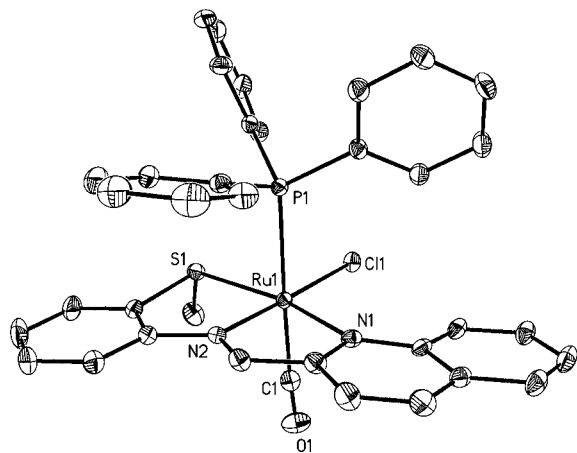

Figure 3. Thermal ellipsoid (50% probability level) plot of $[Ru(Cl)(CO)(qmtpm)(PPh_3)]^+$ (cation of **2**) with the atom-labeling scheme. Hydrogen atoms have been omitted for the sake of clarity.

triphenylphosphine is axially positioned trans to the CO ligand, while Cl⁻ occupies the remaining site, in the same plane as qmtpm. Interestingly, this particular orientation of the ancillary ligands (PPh₃ and Cl) relative to CO in **2** has been noted in another ruthenium monocarbonyl complex $[Ru(Cl)(CO)\text{-}(terpy)(PPh_3)]PF_6$, which features the planar tridentate 2,2′:6′,2″-terpyridine (terpy) ligand.[30] The Ru−P bond length at 2.4719(7) Å in **2** is slightly longer than those noted in other ruthenium(II) phosphinecarbonyl complexes such as $[Ru(Cl)\text{-}(CO)(PPh_3)(H\text{-}pybox)]BF_4$ [where H-pybox = 2,6-bis-(dihydrooxazolin-2′-yl)pyridine; Ru−P = 2.311(3) Å][31] and $[RuCl(CO)(NN′N)(PPh_3)]OTf$ [where NN′N = 2,6-bis-[(dimethylamino)methyl]pyridine; Ru−P = 2.2384(2) Å].[32] This lengthening of the Ru−P bond is expected because, unlike these latter carbonyl complexes, the PPh₃ ligand is trans to CO in **2**. The short Ru−C(O) bond distance [1.923(2) Å] and the almost linear Ru−C(O) bond angle are both typical of ruthenium(II) phosphinecarbonyl complexes.[30,31]

3. The structure of the cation of **3** is shown in Figure 4, and the selected structural parameters are listed in Table 2. Here
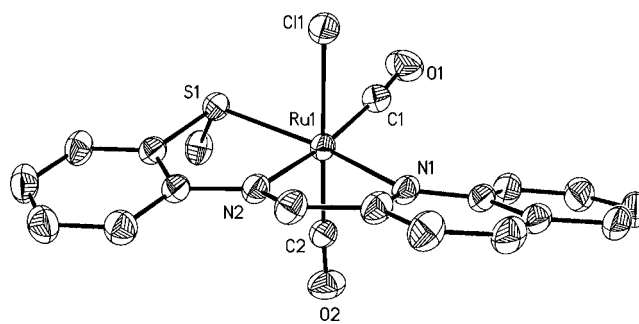

Figure 4. Thermal ellipsoid (50% probability level) plot of $[Ru(Cl)(CO)_2(qmtpm)]^+$ (cation of **3**) with the atom-labeling scheme. Hydrogen atoms have been omitted for the sake of clarity.

again the qmtpm ligand is bound to the Ru^II center in a meridional fashion. The two bound CO molecules are cis to each other, while one Cl⁻ ligand occupies an axial site. The Ru−Cl bond distances in **2** and **3** are similar [2.4352(6) Å vs 2.4176(7) Å] regardless of their coordination with respect to the imine nitrogen atom of qmtpm (in **2**) versus CO (in **3**). The Ru−C(O) bond distances in **3** are almost identical [1.903(3) and 1.890(3) Å], suggesting a uniform extent of back-bonding between the CO ligands and the metal center. Such Ru−C(O) bond lengths and the linearity of the corresponding bond angles (∠O2−C2−Ru1: 175.6°) have been observed in other *cis*-ruthenium(II) dicarbonyl complexes such as $[Ru(CO)_2(mnt\text{-}\kappa^2SS')(terpy\text{-}\kappa^2NN')]$ (where mnt-

κ^2SS' = maleonitriledithiolate and terpy-κ^2NN' = 2,2':6',2''-terpyridine).[33]

5. The structure of the cation of **5** (shown in Figure 5) reveals meridional binding of the qmtpm ligand to the Ru[II]
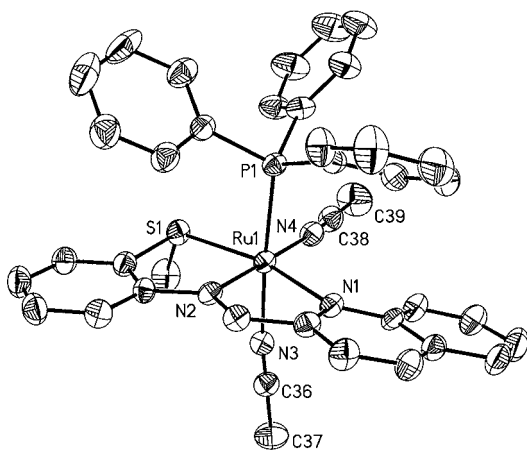

Figure 5. Thermal ellipsoid (50% probability level) plot of [Ru(MeCN)$_2$(qmtpm)(PPh$_3$)]$^+$ (cation of **5**) with the atom-labeling scheme. Hydrogen atoms have been omitted for the sake of clarity.

center of this complex. Two MeCN molecules (cis to each other) and a PPh$_3$ ligand complete the octahedral coordination around the Ru[II] center. Much like in **2**, the triphenylphosphine ligand is perpendicular to the qmtpm plane. The Ru−P bond

length at 2.3485(19) Å (Table 2) falls in the range of known ruthenium(II) triphenylphosphine complexes.[31,32] The Ru−N$_{acn}$ (acn = acetonitrile) bond lengths of **4** [2.056(6) and 2.087(6) Å] are slightly longer than those observed in other ruthenium bis(acetonitrile) complexes such as [Ru(Cl)(MeCN)$_2$)(L)(PPh$_3$)]Cl [where L = 2-(2-pyridyl)-benzothiazole; Ru−N$_{acn}$ = 1.97(13) and 2.01(12) Å].[34]

Spectroscopic Properties. All of the ruthenium complexes reported herein are diamagnetic in the solid state and in solution, as evidenced by their clean ^{1}H NMR spectra. For example, the ^{1}H NMR spectrum of **2** in CDCl$_3$ is shown in Figure 6. Ligation of the thioether end of the qmtpm ligand to the Ru[II] center is confirmed by the downfield shift of the SCH$_3$ signal from 2.52 ppm in the free ligand to 3.08 and 2.90 ppm in **2** and **5**, respectively. Interestingly, **3** exhibits two resonances for the SCH$_3$ unit (3.02 and 3.14 ppm) presumably because of two distinct orientations of this group with respect to the planar qmtpm ligand in solution. In its Fourier transform infrared spectrum, **2** exhibits one strong ν_{CO} band at 2028 cm^{-1}, similar to [Ru(Cl)(CO)(terpy)(PPh$_3$)]PF$_6$.[30] As expected, the dicarbonyl complex **3** displays two strong ν_{CO} bands at 2086 and 2038 cm^{-1}.[31,33]

The EAS spectra of **2**, **4**, and **5** all exhibit one strong MLCT band in the visible region (Figure 7). These signature spectra allow one to readily identify the products of interconversions outlined in Scheme 1. For example, when **2** is heated in acetonitrile in the presence of AgClO$_4$, formation of **5** is readily evidenced by a shift of the absorption maximum of the 460 nm band to 495 nm. Similarly, loss of CO from **2** in acetonitrile
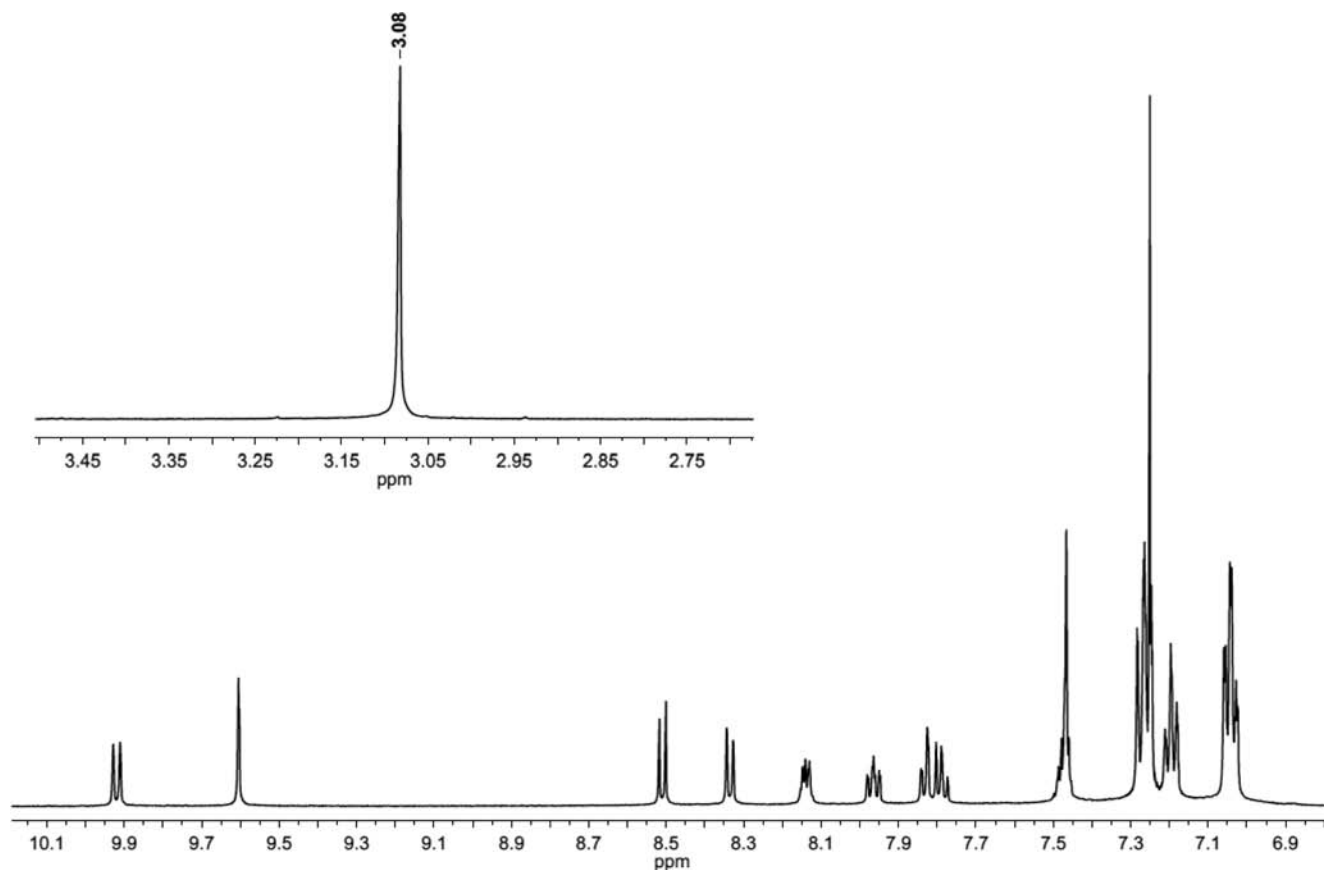

Figure 6. Partial (7−10 ppm) ^{1}H NMR (500 MHz) spectrum of **2** in CDCl$_3$ at 298 K. The resonances of the 11 protons of the qmtpm ligand are spread out in the 7.4−10 ppm region, while peaks for the PPh$_3$ protons appear between 7 and 7.3 ppm. Inset: Resonance of the −SMe at 3.08 ppm.
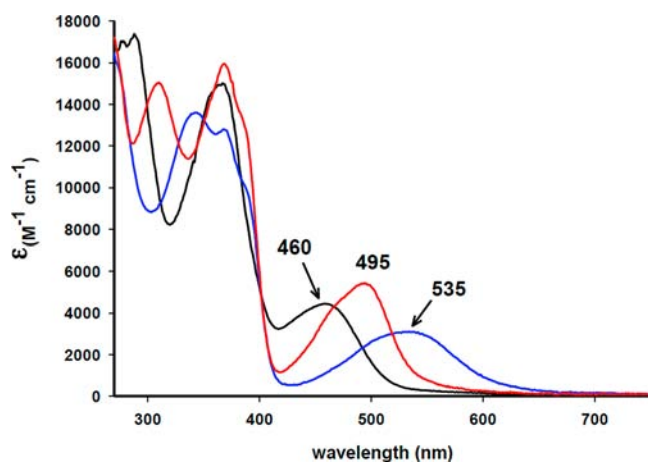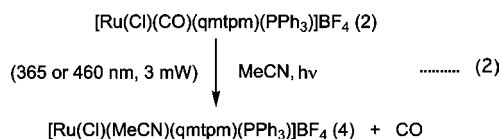
Figure 7. EAS spectra of **2** (black trace), **4** (blue trace), and **5** (red trace) in acetonitrile.

Figure 8. Changes in the absorption spectrum of **2** upon exposure to 365 nm light (power = 10 mW/cm^2).

upon illumination (vide infra) leads to a shift of λ_{max} from 465 to 535 nm, indicating formation of **4**. It is interesting to note that the typical blue (for **1**), magenta (for **4**), or red (for **5**) colors of the Ru^{II}qmtpm complexes are lost upon coordination of one or two CO ligand(s). For example, coordination of one CO to **1** changes the deep-blue color (λ_{max} = 610 nm) to orange-yellow (λ_{max} = 460 nm; Figure 5). Likewise, **3** with two bound CO ligands exhibits its λ_{max} at 385 nm (yellow). As described in a forthcoming section, DFT studies have provided insight into such changes in the MLCT bands of these complexes.

Photorelease of CO in Solution. When a solution of **2** in ethanol or chloroform is kept in the dark, no change is noted with time. However, solutions of **2** in acetonitrile show small changes in its absorption spectrum over hours because of the slow replacement of CO with acetonitrile. The strong affinity of acetonitrile toward Ru^{II} centers as well as the strong trans-labilizing effect of the PPh$_3$ ligand promotes such CO loss. This behavior has also been reported for [Ru(Cl)(CO)(terpy)-(PPh$_3$)]PF$_6$ under similar conditions.[30] As expected, **3** with no PPh$_3$ ligand is indefinitely stable in acetonitrile. Quite in contrast to these behaviors, exposure to light brings about rapid changes in the absorption spectra of **2** and **3**. When solutions of **2** or **3** in ethanol or acetonitrile are exposed to 350−500 nm light, the absorption spectrum undergoes rapid changes because of photorelease of CO, as evidenced by reduced myoglobin assay (Figure S2, Supporting Information). Changes in the absorption spectrum of **2** in acetonitrile upon exposure to 365 nm light are shown in Figure 8. Careful inspection of the spectra reveals that **2** is quantitatively converted to **4** (eq 2)

[Ru(Cl)(CO)(qmtpm)(PPh$_3$)]BF$_4$ (2)

(365 or 460 nm, 3 mW) $\Big\downarrow$ MeCN, hν .... (2)

[Ru(Cl)(MeCN)(qmtpm)(PPh$_3$)]BF$_4$ (4) + CO

within 60 min with no apparent decomposition, as evidenced by clean isosbestic points at 490, 400, 380, and 355 nm. Data from myoglobin assay confirm that **2** delivers 1 equiv of CO under such illumination (eq 2). The apparent first-order rate constant of CO release k_{CO} from **2** is faster in acetonitrile than that in ethanol, and the k_{CO} values change with the wavelength of light. For example, in acetonitrile, **2** exhibits k_{CO} values of 0.065 ± 0.001 and 0.0063 ± 0.0002 min^{-1} with visible light
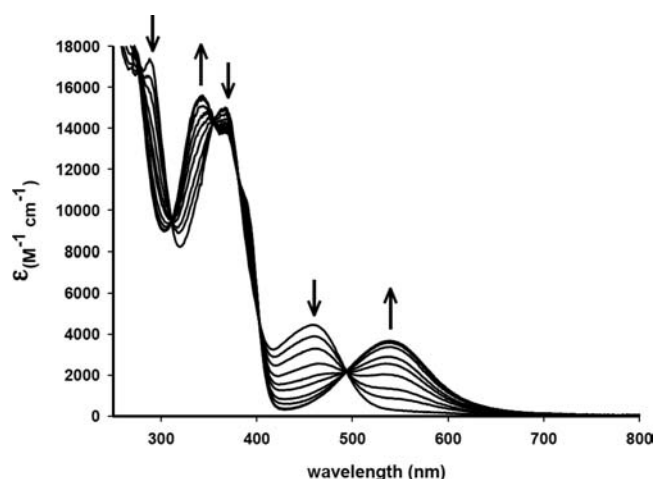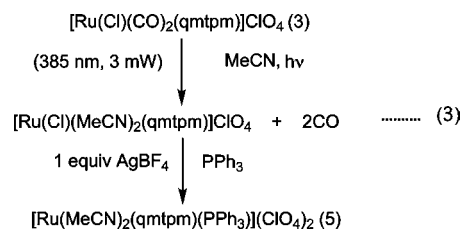
(power = 15 mW/cm^2) with cutoff filters at $\lambda \geq$ 380 nm and $\lambda \geq$ 440 nm, respectively. In ethanol, the k_{CO} values drop to 0.031 ± 0.001 and 0.0032 ± 0.0001 min^{-1} when illuminated with the same light sources. Notable acceleration in CO photorelease from **2** is observed with low-power (5−10 mW/cm^2) UV light. For example, in ethanol, a k_{CO} value of 0.81 ± 0.01 min^{-1} is obtained under 310 nm illumination.

Yellow solutions of **3** in ethanol and acetonitrile release CO upon exposure to light in the 360−300 nm range. For example, when exposed to a narrow-width UV-light source with λ_{max} at 310 nm (power = 7 mW/cm^2), **3** exhibits rapid changes in its EAS spectrum in acetonitrile with isosbestic points at 480, 365, and 300 nm and affords a k_{CO} value of 0.22 ± 0.01 min^{-1}. Because exhaustive photolysis of **3** followed by replacement of the Cl$^-$ ligand with PPh$_3$ affords **5** quantitatively (eq 3), it is

[Ru(Cl)(CO)$_2$(qmtpm)]ClO$_4$ (3)

(385 nm, 3 mW) $\Big\downarrow$ MeCN, hν

[Ru(Cl)(MeCN)$_2$(qmtpm)]ClO$_4$ + 2CO .... (3)

1 equiv AgBF$_4$ $\Big\downarrow$ PPh$_3$

[Ru(MeCN)$_2$(qmtpm)(PPh$_3$)](ClO$_4$)$_2$ (5)

evident that **3** delivers 2 equiv of CO under exposure to 310 nm light. When λ_{max} of the light source is shifted to 325 nm, the value of k_{CO} drops to 0.08 ± 0.01 min^{-1}, again showing the dependence of k_{CO} on the wavelength of light.

DFT and TDDFT Studies. DFT and TDDFT calculations were performed to obtain the optimized geometries, MO electron densities, and calculated electronic transitions for **2**−**5**. The primary objective of this study was to identify the electronic transitions that give rise to CO release from photoCORMs like **2** and **3** under illumination. Another major objective was to determine how the auxiliary ligands such as PPh$_3$, MeCN, and Cl$^-$ affect the MLCT transitions and facilitate Ru−CO bond scission. The DFT-optimized structures of **2**, **3**, and **5** show very good agreement with the bond lengths and bond angles observed in the corresponding crystal structure of each complex (Table S1, Supporting Information). The structure of **4** was obtained by exchanging an acetonitrile of **5** with Cl$^-$ followed by optimization.

Table 4. Energies (E, nm) and Oscillator Strengths (f) of the Calculated (TDDFT) Electronic Transitions with the MOs Involved with Each Transition[a]

energy (nm)	oscillator strength	transition
		$[Ru(Cl)(CO)(qmtpm)(PPh_3)]BF_4$ (**2**)
467	0.0489867	$\pi(Ru-CO)-p(Cl)-\pi(Ru-PPh_3) \rightarrow \pi^*(Q-PhS-SB)$
431	0.0566891	$\pi(PPh_3)-\pi(Ru-PPh_3)-\pi(Ru-CO) \rightarrow \pi^*(Q-PhS-SB)$
387	0.0302262	$\pi(Ru-CO-SMe) \rightarrow \pi^*(Q-PhS-SB)$
381	0.0529700	$\pi(PPh_3)-\pi(Ru-CO-SMe) \rightarrow \pi^*(Q-PhS-SB)$
374	0.0289463	$\pi(PPh_3)-\pi(PhS) \rightarrow \pi^*(Q-PhS-SB)$
365	0.2146560	$\pi(Ru-CO-SMe)-\pi(PPh_3)-\pi(PhS) \rightarrow \pi^*(Q-PhS-SB)$
323	0.0339253	$\pi(Ru-Q-SMe-SB)-p(Cl) \rightarrow \pi^*(Q-PhS-SB)$
		$[Ru(Cl)(CO)_2(qmtpm)]ClO_4$ (**3**)
445	0.0275726	$\pi(Q-PhS-SB) \rightarrow \pi^*(Q-SB-PhS)$
408	0.0165650	$\pi(Q-PhS-SB)-\pi(Ru-CO-Cl) \rightarrow \pi^*(Q-SB-PhS)$
396	0.1794866	$\pi(Ru-CO)-p(Cl)-\pi(PhS) \rightarrow \pi^*(Q-SB-PhS)$
387	0.2110407	$\pi(Ru-CO)-p(Cl)-\pi(PhS) \rightarrow \pi^*(Q-SB-PhS)$
370	0.0729107	$\pi(Ru-SMe-CO)-\pi(PhS)-p(Cl) \rightarrow \pi^*(Q-SB-PhS)$
		$[Ru(Cl)(MeCN)(qmtpm)(PPh_3)]BF_4$ (**4**)
589	0.0139661	$\pi(Ru-SMe-MeCN-Cl) \rightarrow \pi^*(Q-PhS-SB)$
539	0.0442363	$\pi(Ru-Cl-SMe-MeCN)-\pi(Q) \rightarrow \pi^*(Q-PhS-SB)$
414	0.0384803	$\pi(Ru-PPh_3) \rightarrow \pi^*(Q-PhS-SB)$
391	0.0905007	$\pi(Ru-Cl-PPh_3)-\pi(Q) \rightarrow \pi^*(Q-PhS-SB)$
382	0.0434632	$\pi(PPh_3)-\pi(Ru-SB) \rightarrow \pi^*(Q-PhS-SB)$
370	0.0384393	$\pi(Ru-PPh_3) \rightarrow \pi^*(Q-PhS-SB)$
365	0.0147778	$\pi(Q)-\pi(Ru-PPh_3) \rightarrow \pi^*(Q-PhS-SB)$
357	0.0790384	$\pi(Ru-PPh_3-SMe)-p(Cl) \rightarrow \pi^*(Q-PhS-SB)$
353	0.0131655	$\pi(Ru-PPh_3-SMe)-p(Cl) \rightarrow \pi^*(Q-PhS-SB)$
350	0.0223908	$\pi(PPh_3) \rightarrow \pi^*(Q-PhS-SB)$
342	0.0602548	$\pi(PPh_3)-\pi(Sme) \rightarrow \pi^*(Q-PhS-SB)$
		$[Ru(MeCN)_2(qmtpm)(PPh_3)]ClO_4$ (**5**)
449	0.0787027	$\pi(Ru-MeCN-PPh_3) \rightarrow \pi^*(Q-SB-PhS)$
378	0.0210149	$\pi(Ru-Q-PPh_3) \rightarrow \pi^*(Q-SB-PhS)$
375	0.0685953	$\pi(Ru-PPh_3)-\pi(PhS) \rightarrow \pi^*(Q-SB-PhS)$
357	0.0148138	$\pi(Ru-PPh_3) \rightarrow \pi^*(Q-SB-PhS)$
347	0.2105311	$\pi(PPh_3-PhS)-\pi(Ru-SB) \rightarrow \pi^*(Q-SB-PhS)$
329	0.0473331	$\pi(Ru-PhS-SMe) \rightarrow \pi^*(Q-SB-PhS)$

[a]Orbitals with greater contributions are listed first.

As stated above, the transformations of Scheme 1 are accompanied by sharp changes in color. For example, the replacement of one Cl⁻ (a strong σ donor) of **1** with CO (an excellent π acceptor) results in a loss of the deep-blue color and formation of **2** (pale orange), while the replacement of CO of **2** with acetonitrile (a weak π acceptor) changes the color to deep magenta, indicating formation of **4** (Scheme 1). Similarly, loss of the two CO ligands from **3** (pale yellow) with acetonitrile affords a purple solution of $[Ru(Cl)(MeCN)_2(qmtpm)]^+$ (λ_{max} = 565 nm), which upon replacement of the Cl⁻ with PPh₃ (a good π acceptor) turns deep red because of formation of **5**. TDDFT studies were utilized to gain insight into the nature of transitions that lead to these drastic color changes observed upon CO addition or loss to the $[Ru(qmtpm)]$ frame along with variation in the auxiliary ligands PPh₃, MeCN, and Cl⁻.

The calculated electronic transitions of **2−5** with oscillator strengths above 0.0139 were collected, and those with energies falling within the range of 700−300 nm for each complex are presented in Table 4. As shown in Figure 9, the theoretical electronic spectrum of **2** is in good agreement with the experimental spectrum obtained in acetonitrile. Complex **2** exhibits two major bands in the 300−500 nm region, namely, the MLCT band at 460 nm and a stronger absorption at 370 nm. TDDFT results indicate that, for **2**, two theoretical
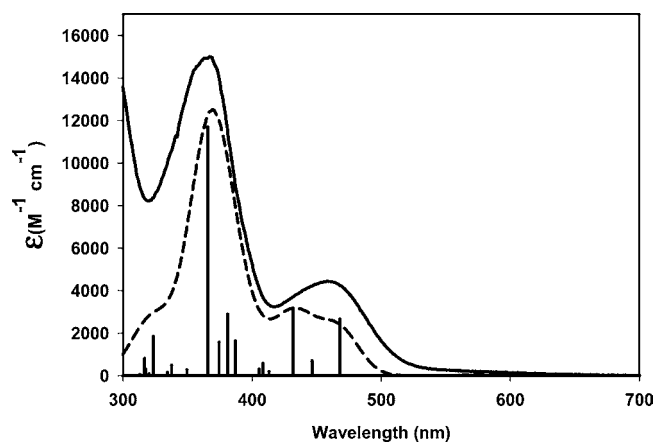

Figure 9. Experimental (solid line) and calculated (dashed line) EAS spectra of **2**.

transitions that occur in the ∼450 nm region are HOMO−1 → LUMO (462 nm) and HOMO−3 → LUMO (431 nm). The 370 nm band corresponds to the theoretical transition with the highest oscillation strength at 355 nm along with a few weaker transitions (Figure 9). Close inspection of the MO energy diagram (Figure 10) displaying the electron densities of the
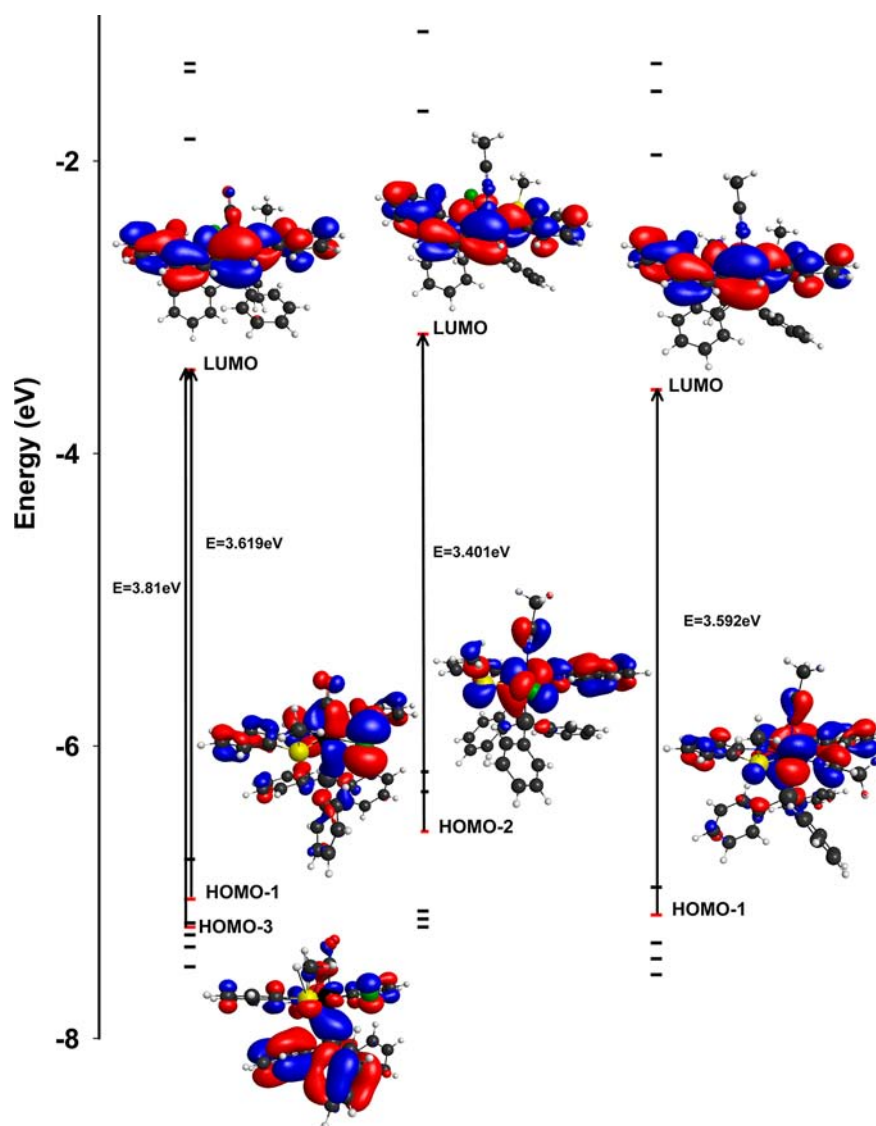
Figure 10. Calculated HOMO/LUMO energy diagrams of **2**, **4**, and **5** (left to right). The most prominent MOs involving transitions under the low-energy band and their diagrams are shown.

MOs that comprise these levels reveals that HOMO−1 is mostly π(Ru−CO) bonding in character mixed with a moderate π(Ru−PPh$_3$) contribution while HOMO−3 is mainly π(Ru−PPh$_3$) with modest π(Ru−CO) participation. The LUMO, on the other hand, is mostly composed of the ligand frame consisting of the π^* orbital of the quinoline, the imine functionality, and the π^* orbital of the Ph(SMe) unit. It is important to note that exposure to visible light ($\lambda \geq 440$ nm) causes moderate CO photorelease from **2**. The TDDFT results strongly suggest that such Ru−CO bond labilization arises from a shift of the electron density from the Ru−CO moiety to the ligand frame. Partial reduction in Ru−PPh$_3$ back-bonding also occurs during the 431 nm transition. The much faster photorelease of CO from **2** upon exposure to light of $\lambda \geq$ 380 nm stems from the predicted HOMO−9 → LUMO transition at 365 nm (Figure 9). Interestingly, HOMO−9 also has a strong π(Ru−CO) character in addition to a moderate contribution from the quinoline π orbital (not shown in Figure 10). Transfer of the electron density from this orbital to the LUMO therefore results in accelerated CO release. Taken together, these results suggest that transitions shifting the electron density from the π(Ru−CO) moiety to the ligand frame promote CO release from photoCORMs like **2**.

The photoproduct **4** exhibits its MLCT band at 535 nm (Figure 7). TDDFT results predict a theoretical HOMO−2 → LUMO transition at 588 nm and a comparatively stronger HOMO−3 → LUMO transition at 538 nm. As is evident from Figure 10, the replacement of CO with MeCN (a moderate π acceptor) raises the energies of the occupied MOs while the LUMO (mostly comprised of the π^* orbitals spread over the qmtpm ligand frame) is minimally affected. This effect is clearly reflected in the change of color from orange-yellow (for **2**) to magenta (in **4**) upon CO photorelease. Replacement of Cl$^-$ of **4** with MeCN (a moderate π acceptor), on the other hand, stabilizes the HOMO−1 in addition to slightly lowering the LUMO in the case of **5**. The combined effect of such an alteration leads to a net increase in the transition energy (from 3.401 to 3.592 eV; Figure 10), as reflected in the color change from magenta (in **4**) to deep red (in **5**).

As described above, the dicarbonyl complex **3** exhibits CO photorelease with UV light. The calculated MOs involved in the electronic transitions of **3** are displayed in Figure 11
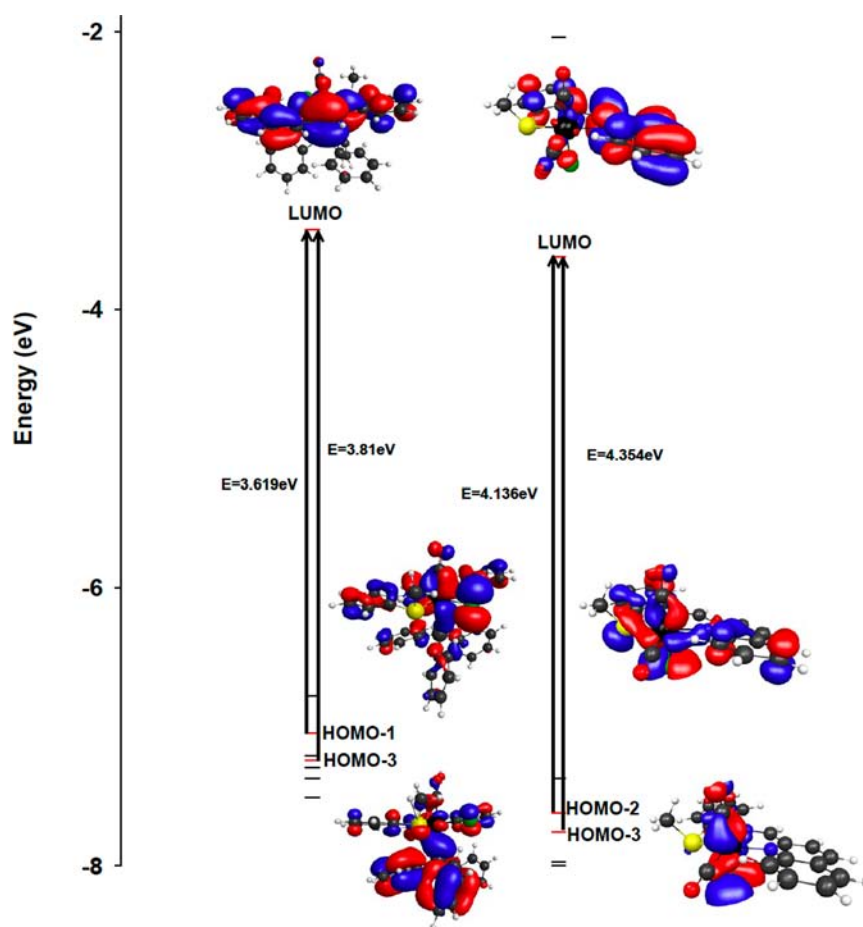
Figure 11. Calculated HOMO/LUMO energy diagram of **2** and **3** (left to right). The most prominent MOs involved with transitions under the low-energy band and their diagrams are shown.

alongside those of **2**. TDDFT studies predict that, for **3**, transitions originating from both HOMO−2 and HOMO−3 into the LUMO give rise to the experimental absorption maximum at ∼380 nm (Figure S1, Supporting Information). This HOMO−2/HOMO−3 transition into the antibonding orbitals of the ligand frame (LUMO) again corresponds to a shift in the electron density from the Ru^{II} center to the qmtpm ligand frame, consistent with a MLCT process. Scrutiny of the nature of HOMO−2 and HOMO−3 reveals a combined Ru−Cl and Ru−CO π-bonding character in these occupied orbitals (Figure 11). Placement of Cl$^-$ (a σ donor) trans to CO clearly fosters strong back-bonding interactions between the metal and the CO group. Such favorable interactions must be overcome to promote a shift in the electron density toward the LUMO (mostly ligand π* orbitals). As a consequence, **3** requires UV light for the release of CO.

■ SUMMARY AND CONCLUSIONS

The following are the summary and conclusions of this investigation:

(a) Mono- and dicarbonyl complexes, namely, **2** and **3**, have been synthesized through the careful choice of starting ruthenium(II) sources and the tridentate ligand qmtpm. The crystal structures of these two carbonyl complexes reveal that, unlike the case with the Mn^I center,[20] the ligand qmtpm binds the Ru^{II} center in **2** and **3** in a tridentate (and *meridional*) fashion. In **3**, the two CO ligands are cis to each other.

(b) Although stable in the dark, solutions of **2** and **3** in ethanol, acetonitrile, and dichloromethane are sensitive to light. Both complexes exhibit excellent CO photolability under low-power (5−10 mW) UV light (300−350 nm). In the case of **2**, moderate photorelease of CO is also noted upon exposure to low-power (15−30 mW) visible light in the range 350−480 nm. The results of myoglobin assay have confirmed quantitative CO release in both cases. Loss of CO from **2** followed by replacement of Cl$^-$ (by Ag$^+$) in acetonitrile gives rise to **5** as the photoproduct, which has been characterized by crystallography. Exhaustive photolysis of **3** followed by replacement of the Cl$^-$ ligand with PPh$_3$ also affords **5** quantitatively.

(c) The Results of DFT and TDDFT studies demonstrate that, with both photoCORMs, exposure to light promotes transfer of the electronic charge density from MOs with strong π(Ru−CO) bonding in character to a LUMO comprised of mostly the qmtpm ligand π frame. Such loss of π-back-bonding leads to rapid CO release. An increase in the number of CO ligands in the photoCORMs (going from **2** to **3**) shifts the MLCT bands to higher energy, and as a consequence, **3** requires UV light for CO release. The theoretical results also indicate that the ancillary ligand PPh$_3$ (trans to CO) plays a significant role in the Ru−CO bond labilization process in **2**.

(d) The low-lying LUMOs in **2** and **3**, a direct consequence of the extended conjugation across the imine function and the quinoline moiety (plus the −SMe appendage) of the qmtpm ligand, bring the major electronic transitions to the 350−450 nm range. This fact underscores the importance of designed

11329

dx.doi.org/10.1021/ic4016004 | *Inorg. Chem.* 2013, 52, 11320−11331

ligands for the successful isolation of photoCORMs that are sensitive to visible and near-IR light. Although metal carbonyl complexes derived from typical ligands such as bipyridine and water-soluble phosphines[14] have been shown to release CO upon exposure to UV light, novel ligands that would initiate specific MLCT interactions will be required the isolation of photoCORMs suitable for use in the photodelivery of CO to biological targets.

ASSOCIATED CONTENT

Ⓢ Supporting Information

X-ray crystallographic data (in CIF format) for **2**·H₂O, **3**, and **5**, experimental and calculated elctronic absorption spectra of **3** (Figure S1), traces of spectra showing conversion of reduced Mb to Mb-CO in a typical myoglobin assay experiment (Figure S2), and selected bond distances (Å) and angles (deg) for **2**−**5** with DFT-optimized bond distances and angles (Table S1). This material is available free of charge via the Internet at http://pubs.acs.org.

AUTHOR INFORMATION

Corresponding Author
*E-mail: pradip@ucsc.edu.

Notes

The authors declare no competing financial interest.

ACKNOWLEDGMENTS

REFERENCES

(1) (a) Kikuchi, G.; Yoshida, T.; Noguchi, M. *Biochem. Biophys. Res. Commun.* **2005**, *338*, 558−567. (b) Wu, L.; Wang, R. *Pharmacol. Rev.* **2005**, *57*, 585−630.

(2) (a) Öllinger, R.; Wang, H.; Yamashita, K.; Wegiel, B.; Thomas, M.; Margreiter, R.; Bach, F. H. *Antioxid. Redox Signal.* **2007**, *9*, 2175−2185. (b) Öllinger, R.; Yamashita, K.; Bilban, M.; Erat, A.; Kogler, P.; Thomas, M.; Csizmadia, E.; Usheva, A.; Margreiter, R.; Bach, F. H. *Cell Cycle* **2007**, *6*, 39−43. (c) Fondevila, C.; Shen, X. D.; Tsuchiyashi, S.; Yamashita, K.; Csizmadia, E.; Lassman, C.; Busuttil, R. W.; Kupiec-Weglinski, J. W.; Bach, F. H. *Hepatology* **2004**, *40*, 1333−1341.

(3) (a) Komuro, T.; Borsody, M. K.; Ono, S.; Marton, L. S.; Weir, B. K.; Zhang, Z. D.; Paik, E.; Macdonald, R. L. *Expt. Biol. Med.* **2001**, *226*, 860−865. (b) Zhang, F.; Kaide, J.-I.; Rodriguez-Mulero, F.; Abraham, N. G.; Nasjletti, A. *Am. J. Hypertens.* **2001**, *14*, 62S−67S.

(4) Brouard, S.; Otterbin, L. E.; Anrather, J.; Tobiasch, E.; Bach, F. H.; Choi, A. M. K.; Soares, M. P. *J. Exp. Med.* **2000**, *192*, 1015−1025.

(5) Kim, H. P.; Ryter, S. W.; Choi, A. M. K. *Annu. Rev. Pharmacol. Toxicol.* **2006**, *46*, 411−449.

(6) Vieira, H. L. A.; Queiroga, C. S. F.; Alves, P. M. *J. Neurochem.* **2008**, *107*, 375−384.

(7) (a) Faller, S.; Hoetzel, A. *Curr. Pharmaceut. Biotechnol.* **2012**, *13*, 777−786. (b) Ghosh, S.; Wilson, M. R.; Choudhury, S.; Yamamoto, H.; Goddard, M. E.; Falusi, B.; Marczin, N.; Takata, M. *Am. J. Physiol. Lung Cell Mol. Physiol.* **2005**, *288*, L1003−L1009. (c) Zhang, X.; Shan, P.; Alam, J.; Davis, R. J.; Flavell, R. A.; Lee, P. J. *J. Biol. Chem.* **2003**, *278*, 22061−22070.

(8) (a) Kohmoto, J.; Nakao, A.; Stolz, D. B.; Kaizu, T.; Tsung, A.; Ikeda, A.; Shimizu, H.; Takahashi, T.; Tomiyama, K.; Sugimoto, R.; Choi, A. M. K.; Billiar, T. R.; Murase, N.; McCurry, K. R. *Am. J. Transplant.* **2007**, *7*, 2279−2290. (b) Fujita, T.; Toda, K.; Karimova, A.; Yan, S. F.; Naka, Y.; Yet, S. F.; Pinsky, D. J. *Nat. Med.* **2001**, *7*, 598−604.

(9) (a) Stein, A. B.; Bolli, R.; Dawn, B.; Sanganalmath, S. K.; Zhu, Y.; Wang, O. L.; Guo, Y.; Motterlini, R.; Xuan, Y. T. *J. Mol. Cell. Cardiol.* **2012**, *52*, 228−236. (b) Stein, A. B.; Guo, Y.; Tan, W.; Wu, W. J.; Zhu, X.; Li, Q.; Luo, C.; Dawn, B.; Johnson, T. R.; Motterlini, R.; Bolli, R. *J. Mol. Cell. Cardiol.* **2005**, *38*, 127−134. (c) Otterbein, L. E.; Mantell, L. L.; Choi, A. M. K. *Am. J. Physiol.* **1999**, *276*, L688−L694.

(10) (a) Stein, A. B.; Bolli, R.; Dawn, B.; Sanganalmath, S. K.; Zhu, Y.; Wang, O. L.; Guo, Y.; Motterlini, R.; Xuan, Y. T. *J. Mol. Cell. Cardiol.* **2012**, *52*, 228−236. (b) Stein, A. B.; Guo, Y.; Tan, W.; Wu, W. J.; Zhu, X.; Li, Q.; Luo, C.; Dawn, B.; Johnson, T. R.; Motterlini, R.; Bolli, R. *J. Mol. Cell. Cardiol.* **2005**, *38*, 127−134.

(11) (a) Nakao, A.; Choi, A. M. K.; Murase, N. *J. Cell. Mol. Med.* **2006**, *10*, 650−671. (b) Sato, K.; Balla, J.; Otterbin, L.; Smith, R. N.; Brouard, S.; Lin, Y.; Csizmadia, E.; Sevigny, J.; Robson, S. C.; Vercellotti, G.; Choi, A. M. K.; Bach, F. H.; Soares, M. P. *J. Immunol.* **2001**, *166*, 4185−4194.

(12) (a) Zobi, F. *Future Med. Chem.* **2013**, *5*, 175−188. (b) Romão, C. C.; Blättler, W. A.; Seixas, J. D.; Bernardes, G. J. L. *Chem. Soc. Rev.* **2012**, *41*, 3571−3583. (c) Motterlini, R.; Otterbein, L. E. *Nat. Rev. Drug Discovery* **2010**, *9*, 728−743. (d) Mann, B. E. *Top. Organomet. Chem.* **2010**, *32*, 247−285.

(13) (a) Rimmer, R. D.; Pierri, A. E.; Ford, P. C. *Coord. Chem. Rev.* **2012**, *256*, 1509−1519. (b) Schatzschneider, U. *Inorg. Chim. Acta* **2011**, *374*, 19−23. (c) Schatzschneider, U. *Eur. J. Inorg. Chem.* **2010**, 1451−1467.

(14) Rimmer, R. D.; Richter, H.; Ford, P. C. *Inorg. Chem.* **2010**, *49*, 1180−1185.

(15) Jackson, C. S.; Schmitt, S.; Dou, Q. P.; Kodanko, J. J. *Inorg. Chem.* **2011**, *50*, 5336−5338.

(16) Niesel, J.; Pinto, A.; Peindy N'Dongo, H. W.; Merz, K.; Ott, I.; Gust, R.; Schatzschneider, U. *Chem. Commun.* **2008**, 1798.

(17) (a) Huber, W.; Linder, R.; Niesel, J.; Schatzschneider, U.; Spingler, B.; Kunz, P. C. *Eur. J. Inorg. Chem.* **2012**, 3140. (b) Kunz, P. C.; Huber, W.; Rojas, A.; Schatzschneider, U.; Spingler, B. *Eur. J. Inorg. Chem.* **2009**, 5358. (c) Pfeiffer, H.; Rojas, A.; Niesel, J.; Schatzschneider, U. *Dalton Trans.* **2009**, 4292−4298.

(18) Berends, H. M.; Kurz, P. *Inorg. Chim. Acta* **2012**, *380*, 141−147.

(19) Gonzalez, M. A.; Yim, M. A.; Cheng, S.; Moyes, A.; Hobbs, A. J.; Mascharak, P. K. *Inorg. Chem.* **2012**, *51*, 601−608.

(20) Gonzalez, M. A.; Carrington, S. J.; Fry, N. L.; Martinez, J. L.; Mascharak, P. K. *Inorg. Chem.* **2012**, *51*, 11930−11940.

(21) Stephenson, T. A.; Wilkinson, G. *J. Inorg. Nucl. Chem.* **1966**, *28*, 945−956.

(22) Castro, A. G.; Costa, J. S.; Pievo, R.; Massera, C.; Mutikainen, I.; Turpeinen, U.; Gamez, P.; Reedijik, J. *Z. Anorg. Allg. Chem.* **2008**, *634*, 2477−2482.

(23) Montalti, M.; Credi, A.; Prodi, L.; Gandolfi, M. T. *Handbook of Photochemistry*, 3rd ed.; CRC Press: Boca Raton, FL, 2006.

(24) McLean, S.; Mann, B. E.; Poole, R. K. *Anal. Biochem.* **2012**, *427*, 36−40.

(25) Nemukhin, A. V.; Grigorenko, B. L.; Granovsky, A. A. *Moscow Univ. Chem. Bull.* **2004**, *45*, 75−102.

(26) Miertus, S.; Scrocco, E.; Tomasi, J. *Chem. Phys.* **1981**, *55*, 117−120.

(27) Waller, M. P.; Braun, H.; Hojdis, N.; Bühl, M. *J. Chem. Theory Comput.* **2007**, *3*, 2234−2242.

(28) Hossain, M.; Maji, M.; Chattopadhyay, S. K.; Ghosh, S.; Blake, A. J. *Polyhedron* **1998**, *17*, 1897−1906.

(29) Moreno, M. A.; Haukka, M.; Kallinen, M.; Pakkanen, T. A. *Appl. Organomet. Chem.* **2006**, *20*, 51−69.

(30) Ooyama, D.; Saito, M. *Inorg. Chim. Acta* **2006**, *359*, 800−806.

(31) Cuervo, D.; Ménendez-Pedregal, E.; Díez, J.; Gamasa, M. P. *J. Organomet. Chem.* **2011**, *696*, 1861−1867.

(32) Abbenhuis, R. A. T. M.; del Rio, I.; Bergshoef, M. M.; Boersma, J.; Veldman, N.; Spek, A. L.; van Koten, G. *Inorg. Chem.* **1998**, *37*, 1749−1758.

(33) Sugimoto, H.; Tsuge, K.; Tanaka, K. *J. Chem. Soc., Dalton Trans.* **2001**, 57−63.

(34) Maji, M.; Sengupta, P.; Chattopadhyay, S. K.; Mostafa, G.; Schwalbe, C. H.; Ghosh, S. *J. Coord. Chem.* **2001**, *54*, 13–24.

11331

dx.doi.org/10.1021/ic4016004 | *Inorg. Chem.* 2013, 52, 11320–11331